



Journal Homepage: -www.journalijar.com
**INTERNATIONAL JOURNAL OF
 ADVANCED RESEARCH (IJAR)**

Article DOI:10.21474/IJAR01/6819
 DOI URL: <http://dx.doi.org/10.21474/IJAR01/6819>



RESEARCH ARTICLE

COPPER NANOPARTICLES OBTAINED BY ARC DISCHARGE METHOD: SYNTHESIS, CHARACTERIZATION, AND PROPERTIES.

Ahmed M. El-Khatib¹, Moustafa M. Mohamed², Mohamed S. Badawi³, A. S. Doma⁴, Amna S. Mohamed²
 and A. A. Thabet².

1. Physics Department, Faculty of Science, Alexandria University, PO 21511 Alexandria, Egypt.
2. Department of Medical Equipment Technology, Faculty of Allied Medical Science, Pharos University, Alexandria, Egypt.
3. Department of Physics, Faculty of Science, Beirut Arab University, Beirut, Lebanon.
4. Advanced Technology and New Materials Research Institute (ATNMRI), City for Scientific Research and Technological Applications (SRTA-CITY), Alexandria, Egypt.

Manuscript Info

Manuscript History

Received: 02 February 2018
 Final Accepted: 04 March 2018
 Published: April 2018

Keywords:-

Double arc discharge, Copper nanoparticle, Arc evaporation.

Abstract

Our objective in this paper is to study the effect of the current on the fabrication copper nanoparticles Cu- NPs and its effect on the yield and to investigate a new technique for plasma preparation of nanoparticles. A new instrument, which uses a three-phase current to support a double-arc discharge method for generating the plasma and evaporate the solids, is described. The crystal structure of nanoparticles, which was examined by X-ray diffraction XRD, shows that diffraction peaks for the Cu- NPs indicate that they are crystalline in nature. The morphology of the product was examined by Scanning Electron Microscope (SEM). From the micrograph, it was observed that the nanoparticles size ranges from 44 to 123 nm. The particle size analyzer gives the size distributions with an overall sizing range. The particle size analyzer (PSA) constituents with SEM (the particles size ranges from 30-128 nm). The ultraviolet-visible (UV-Vis) spectrometry contributed to the analysis of size and optical properties of the nanoparticles through each current value (from 30A-110A). Fourier transform infrared (FTIR) spectroscopy analysis (4500 - 500 cm⁻¹) confirmed the presences of Cu- NPs by an appearance of no sharp peaks for any functional group. The developed technique was shown to be suitable for the preparation of Cu- NPs of different sizes. However, a scale-up of production rate often leads to an increase in particle size and broadening of size distribution.

Copy Right, IJAR, 2018,. All rights reserved.

Background:-

Scaling up metal nanoparticle production is a desired goal of much research. The need of the industry due to the growing market of applications increases significantly. The double arc discharge technique is one of the most powerful methods available for preparing the Cu NPs. This review will be helpful for the design of new methods for nanomaterial synthesis [1, 2]. The success of double arc discharge technique depends on the method of two arcs working together producing nanoparticles at the same time. There is a significant interest in the synthesis and

Corresponding Author:- A. S. Doma.

Address:- Advanced Technology and New Materials Research Institute (ATNMRI), City for Scientific Research and Technological Applications (SRTA-CITY), Alexandria, Egypt.

applications of Cu NPs [3, 4]. Arc discharge is considered one of the most physical techniques being used. It comprises of various areas of research [5, 6].

In general, the ignition of an electric discharge in the gas or liquid phase leads to the generation of non-thermal plasma, which can be utilized in various processes and technologies. The resulting plasma is formed by various charged particles, especially high energetic electrons, ions and radicals. Arc discharge: This type of discharge is visible and can be thermal or non-thermal. It was measured in a lightning : (a) Non-thermal region: ($0.1 \leq I < 10A$) and (b) Thermal region: ($I \geq 10A$).

The arc discharge in the thermal region is the operating principle of electric switchers. It is also involved in material processing which based on energy transfer such as plasma cutting, thermal plasma spray and welding. According to this description, it can be argued that electric arc welding is in the frame of cold plasma and the discharge type is the thermal arc discharge [7]. In this article, regarding the formation of Cu NPs from the double arc discharge of three rods in water. Formation of uniform Cu NPs via a solid-liquid phase double arc discharge process was reported [8]. Water introduced as the medium of choice by many reports which includes our recent account of media effects on double arc fabrications of nanoparticles. The electric double arc evaporation under liquid surface is the most efficient method for the direct fabrication of Cu NPs through formation of dense metal vapor-clouds which condensed immediately by low liquid temperature [9]. In this manuscript we adopt deionized water for probing the effects of current (30–110 A) on the arc fabrications of Cu NPs. It is found that density of current is a key factor for the morphology, controlling particle sizes, and yields of Cu NPs. Increasing the current can cause an increasing in the particle sizes and yields of Cu NPs production. The advantages which were originated from the double arc discharge process might be promising for opening a new pathway versatile enough to synthesize various metal nanostructures [10].

Double arc discharge is a non-traditional concept of machining which has been widely used to produce nanoparticles. Present work demonstrates synthesis of Cu NPs by double arc discharge method and studies the morphological and optical properties of produced samples. Arc current was selected as an effective parameter for controlling the size and provided a way to adjust the physical properties of synthesized nanoparticles. Several experimental studies have been attempted to improve the control of the arc synthesis process with limited success [11, 12]. A lot of efforts have been held on synthesis of metal nanoparticles for controlling the surface Plasmon resonance [13]. Two types of physical and chemical methods can be used for synthesis of metal nanoparticles. Arc discharge is selected among these types due to its special advantages. Arc discharge in gases has been extensively used for synthesis of various nanostructures but recently liquid environment is developed. Preparation of nanostructures by arc discharge in liquid is cheap and simple because it needs no vacuum equipment, no reactive gas and no heat exchanging system [14, 15]. Significant efforts have been made to understand the synthesis of nanoparticles in thermal single arcs [16]. However, especially when large amounts of metal powder are produced by arc synthesis, micron-sized particles are produced instead of nanoparticles [17]. Increasing evaporation rates lead to bigger primary particles and broader agglomerate size distributions. Different methods to manipulate the particle sizes in single arcs synthesis have been investigated [18], e.g., quenching by dilution [19] or the reduction of power input [20]. Also, the carrier gas composition influences the primary particle size significantly [21]. This work describes the development of a production process for metal nanoparticles based on the double arc discharge synthesis. It contains the development of the single arc discharge systems. In the experiment we tried to develop the method of discharge in liquid, which had been successfully applied to the synthesis of copper to be double arc discharge method working together. The double arc electrodes were evaporated under the effect of current at different values and showing different effects for the morphology and the yield of the produced Cu NPs also the impact of current on the metal NPs have been discussed.

Methods:-

Set up Preparation of Cu- NPs:-

A Schematic diagram of the arc discharge method is shown in Fig. 1 depicts the structure of this work and the connections between the two arcs, Double-arc discharge: The major constituents of this plasma system are (i) three-phase power supply, (ii) double arc discharge structure.

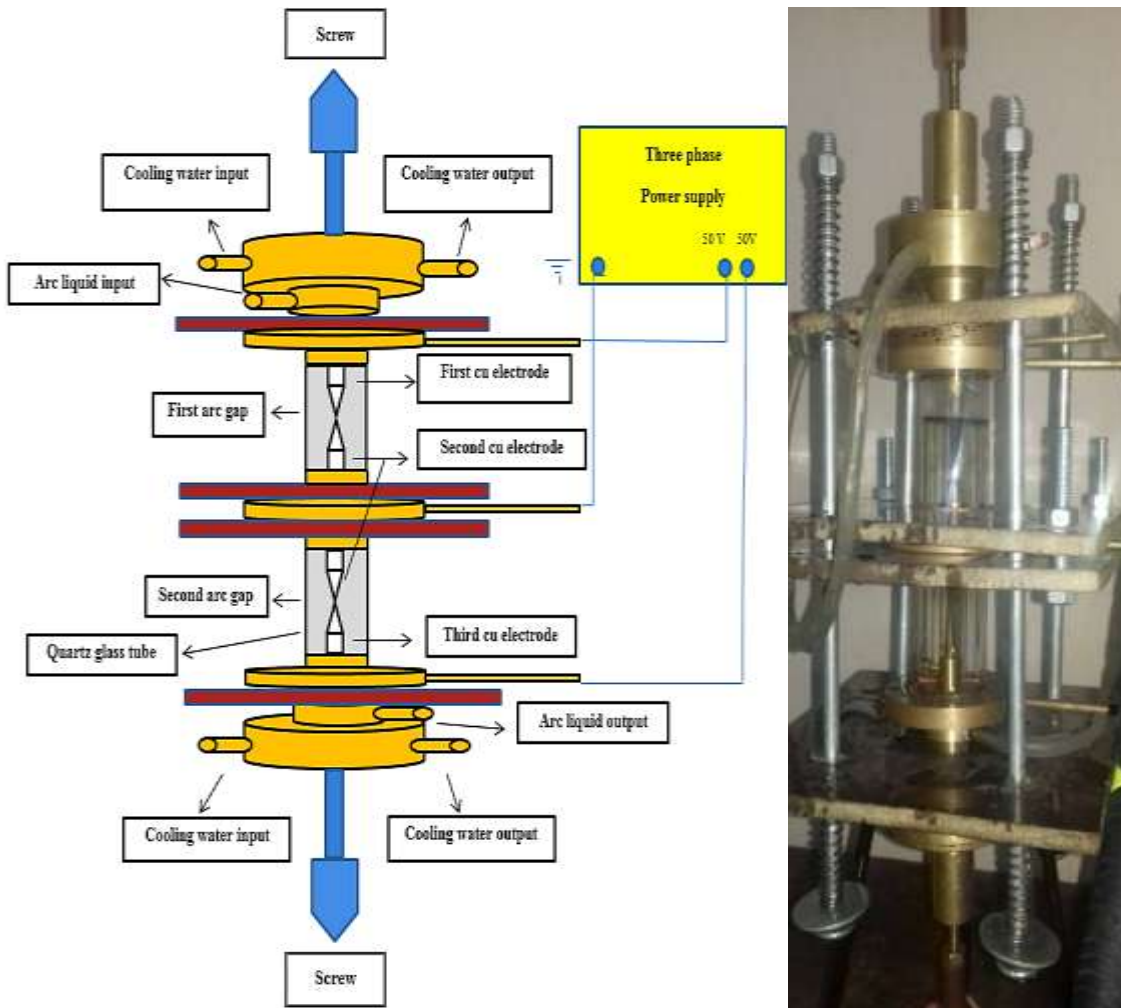


Fig.1:- Three-phase double arc discharge system

The present method requires only an alternating current (AC) three phase power supply and commercially available copper rods. It has a double-walled construction which allows water-cooling. The alternating discharge between the three electrodes has been applied for producing Cu- NPs. The arc discharge was operated between the end surfaces of three copper metal electrodes in dielectric liquid (deionized water). The high purity copper electrodes (99.99%) with a “pencil”-shape structures have the diameters of 7mm and lengths of 25mm were used. The three electrode shapes are shown in Fig. 2 and the inter electrode gaps was 1 mm which translated by hand. Different currents (30A, 50A, 70A, 90A and 110 A) are passed through water submerged copper electrodes (10 minutes). The arc discharge was initiated by the slowly movement of the terminal electrodes (first and third Cu electrode) to the central electrode (second Cu electrode). Consequently, the gap is controlled at approximately 1mm to maintain a stable discharge current and average voltage of 50 volt for each single arc circuit and pulsed arc-discharge was observed at the gap in the liquid phase. The operation parameters are summarized in Table-1.



Fig. 2:- The shape of electrodes

Table 1:- Experimental conditions of particle synthesis experiments

Item	Condition
Arc current (A)	30 A, 50 A, 70 A, 90 A and 110 A
Arc gaps lengths	1 mm
Arc volt	50 V
volume of dielectric liquid	200 ml
The two arcs timing	10 minutes

After all these parameters establishing The Cu electrodes are heated by the high temperature of the arc, the heating source produces an arc with high temperature to melt the metal rods. The rods are melted and vaporized in the region where the arc is generated. Thus, the vaporized metal in the chamber undergoes nucleation, growth and condensation [22], and finally turning into nanoparticles dispersed in deionized water. The low temperature deionized water can condense the submerged metal particles immediately and effectively. The growth rate of the nucleus is controlled by the concentration of the vaporized metal and the temperature of the medium [23].

XRD Analysis

X-ray diffraction (XRD) is a powerful nondestructive technique for characterizing crystalline materials. (XRD) (Shimadzu XRD-6100) provides information on structures; phases, preferred crystal orientations-ray diffraction peaks are produced by constructive interference of a monochromatic beam of X-rays scattered at specific angles from each set of lattice planes in a sample. The peak intensities are determined by the distribution of atoms within the lattice. Consequently, the X-ray diffraction pattern is the fingerprint of periodic atomic arrangements in each material [24]. Other structural parameters, such as average grain size, the crystalline sizes of the CuNPs were calculated by means of an X-ray line broadening method using the Scherrer equation [25]:

$$D = \frac{K\lambda}{\beta \cos\theta} \quad (1)$$

where D is the crystallite size, K is the shape factor, being equal to 0.9, λ is the wavelength of incident X-ray radiation (1.5404 Å for CuK α), β line broadening (FWHM) of the diffraction peak, and θ is the Bragg diffraction angle in degree. The value of d the interplanar spacing between the atoms and the expected 2θ positions is calculated using Bragg's Law:

$$n\lambda = 2d\sin\theta, \quad (2)$$

where θ is the angle of incidence, d is the distance between atomic layers in a crystal, the variable λ is the wavelength of the incident X-ray beam and n is an integer [26]. The distance d is defined by

$$1/d^2 = \frac{K^2+h^2+l^2}{a^2}, \quad (3)$$

where a is unit cell parameter, (h k l) are miller indices. The density of Cu NPs can be calculated through the following equation:

$$\rho = \frac{nA}{a^3 N_A}, \quad (4)$$

where A is the atomic weight of Cu and N_A Avogadro's number ($6.022 \times 10^{23} \text{ mol}^{-1}$).

SEM Analysis:-

Scanning electron microscopy SEM is one of the most powerful methods for determining the critical performance defining attributes. SEM (JEOL JSM-6360 LA), Energy dispersive X-ray spectroscopy (EDX) are used for depiction crystalline structure, morphology, and size of Cu NPs. SEM is incredibly versatile utilizing Technique in characterizing the size, morphology and composition of nanoparticles. SEM may offer better performance for surface and shape analysis, for many nanotechnology developers looking at fundamental size and shape properties, SEM may offer a more productive path to high quality analysis. In this study, the acceleration voltage was set to 10 KV and the working distance was adjusted to around 3mm. SEM is giving morphological examination with direct visualization. The techniques based on electron microscopy offer several advantages in morphological and sizing analysis; however, they provide limited information about the size distribution and true population average. For SEM characterization, nanoparticles solution should be first converted into a dry powder, which is then mounted on a sample holder followed by coating with a conductive metal, such as gold, using a sputter coater. The sample is then scanned with a focused fine beam of electrons. The surface characteristics of the sample are obtained from the secondary electrons emitted from the sample surface [27]. In comparison to the use of scanning probe techniques, mapping the extent of nanoparticle composition is becoming a routine process in the SEM due to the complementary spectroscopic techniques of Energy Dispersive X-ray spectroscopy EDX spectroscopy [28].

Particle Size Analyzer (PSA):-

Particle size distribution is one of the most important parameters of characterization of nanoparticles. The primary particle size determined for different applied electric currents by (N5 Submicron Particle Size Analyzer), according to the production rate. Smaller particles offer larger surface area. The population of the nanoparticles in a powder, as described by its particle size distribution (PSD), affects the properties of a powder and dispersions in many important ways. As a drawback, smaller particles tend to aggregate during storage and transportation of nanoparticle dispersion. Hence, there is a compromise between a small size and maximum stability of nanoparticles [29]. It is possible to extract the average range of the size distribution. The particles have different sizes and distribution patterns based on the current values (30A-110A) to develop deep understanding for correlation between material properties and fabrication parameters.

Optical Properties of Cu NPs:-

(UV-Vis) spectrophotometers are widely used by many laboratories – including those found in academia and research as well as industrial quality assurance. As with wavelength accuracy testing, either solutions or glass/quartz filters can be used. The technique is mainly used quantitatively (although some qualitative analysis can also be performed). UV-Vis absorption spectra were registered on the spectrophotometer (T80+UV/VIS spectrometer) in the wavelength range of 200-1100 nm. All measurements were made at normal conditions. UV considered one of the strategies that are relevant characterization techniques and would be helpful to study the optical properties of the obtained colloidal Cu NPs solutions. It is useful method to represent the energy gaps values of Cu NPs that are attributed to the charge transfer transitions. The UV-Vis absorption spectra of the Cu NPs at each current (30A-110A) were measured in order to investigate the optical energy gaps of the samples. In UV-Vis, high energy electromagnetic radiation in the wavelength range of 100-1100 nm is utilized to promote electrons to higher energy orbitals. The fundamental absorption, which corresponds to electron excitation from the valence band to the conduction band, can be used to determine the value of the optical energy gap. The relationship between the absorption coefficients α and the incident photon energy $h\nu$ can be written as Tauc equation, [30]:

$$\alpha h\nu = B(h\nu - E_g)^n, \quad (5)$$

where B is a constant, E_g is the optical energy gap, h is Planck's constant ($h = 6.626 \times 10^{-34}$ J.s) and n is an exponent which describes the type of the electronic transition. In (5), the absorption coefficient α could be calculated by using Beer Lambert law equation. For $n = 1/2$, we have allowed direct electronic transition whereas for $n = 2$ the case is an indirect electronic transition [31]:

$$I = I_0 e^{-\alpha t}, \quad (6)$$

where t is the thickness of the sample in meter, I is the light intensity after it passes through the sample, I_0 is the initial light intensity; the absorption coefficient can be calculated as follows:

$$\alpha = \frac{2.303A}{t}, \quad (7)$$

where A is the absorbance. To determine the optical Energy gap, we plotted the modified Kubelka–Munk function, i.e., which is a plot between $h\nu$ as x-axis and $(\alpha h\nu)^n$ as y-axis, [32, 33].

Plasmonic Properties of Cu NPs:-

Metal nanostructures are among the most studied nanomaterials due to their outstanding size dependent properties. In particular, nanoparticles of metals show an interesting optical behavior known as size dependent surface plasmon resonance (SPR) as the nanoparticle diameter becomes comparable with, or smaller than the wavelength of incident light [34, 35]. Pioneered by the works of Mie [36] and Ritchie [37] for small particles and planar interfaces respectively, plasmonic developed into widely studied area of condensed matter physics.

The optical properties of metallic nanostructures are determined by strong interactions between the incident light and the conduction electrons. Collective oscillations of the conduction electron gas are called plasmons. At the resonance frequency, such collective electron oscillations may result in the enhancement of electric fields in the vicinity of a nanostructured metallic surface. Therefore, surface plasmons have opened an avenue towards the possibility to amplify, concentrate and manipulate light at nanoscale [38]. The expressions for the spatial profile of the propagating waves inside the two media are based on the geometry depicted in Fig.3.

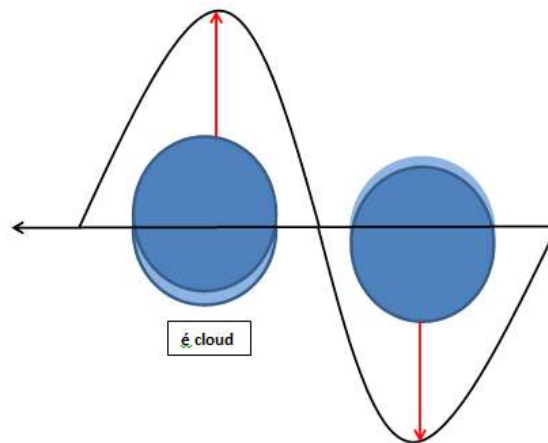


Fig.3:- Plasmon oscillations in metal spheres induced by an electromagnetic wave.

Consequently, represent an oscillator, whose behavior is defined by the electron density and the geometry of the particle. Throughout this text the nanoparticles' resonances are called surface plasmons on metal nanoparticles.

Fourier-Transform Infrared Spectroscopy (FTIR):-

Nanoparticle surfaces need to be studied and understood. And a variety of techniques are available for this purpose. However, one technique in particular that offers several benefits is FTIR spectroscopy. The main advantage of this

technique is you can gain valuable insight into the functional groups of a particular system. FTIR spectra were obtained with FTIR-8400S SHIMADUZ, FTIR spectrophotometer, KBr disc method, and was used in order to study the structures Cu NPs. The functional group present in the Cu NPs solutions was confirmed by FTIR analysis. This means that IR spectroscopy is ideal for observing the vibrational transitions of self-assembled functional groups coordinated to nanoparticle surfaces, and both qualitative and quantitative analysis are possible. Of course, like most analytical techniques, FTIR spectroscopy works best when combined with other methods, and can serve as a wonderful complement to UV-Vis spectroscopy. This is because every technique has specific advantages and drawbacks. By combining such techniques, it's possible to collect detailed information on the interface between the functionalized nanoparticle surface and the surrounding environment [39]. FTIR (in the range of $100\text{--}1100\text{ cm}^{-1}$) was used in order to study the structures of CuNPs. The formation of Cu NPs was confirmed by Fourier-transform infrared spectroscopy (FTIR).

Results and Discussion:-

XRD Calculations:-

XRD study is most important tool used in NM science. A discussion about simple and low cost preparation of Cu NPs and its X-ray diffraction (XRD) studies are presented in this study. Preparation of uniformed Cu NPs size 34 nm, in a normal room temperature is importance of this study. Its XRD analysis confirms the result. XRD measurement is performed in order to determine the primary particle size and composition of the synthesized Cu NPs particles, it is performed to confirm the achieved results. XRD is an easy tool to determine the size and the shape of the unit cell for any compound. Its XRD and SEM results show pure Cu NPs. Hence, Cu NPs, formed in deionized water, at 30A show XRD lines (111), (200), and (220) at $2\theta = 43.05^\circ, 50.18^\circ, 73.88^\circ$, respectively. In Fig.4 diffraction peaks can be indexed to those of pure face centered cubic (f.c.c.) Cu (JCPDS, File No. 04-0836). The observation of diffraction peaks for the Cu NPs indicates that these are crystalline in nature. The nanoparticles synthesized were found to be phase-pure copper without any impurity phase. The XRD peak positions are consistent with metallic copper. Peaks are very sharp due to the high nanocrystalline nature of copper. From this study, considering the peak at degrees, average particle size has been estimated by using Debye - Scherrer formula. The average sizes of the nanoparticles are shown in the Table2. According to Debye Scherrer equation the average particle size was found to be 32.97 nm.

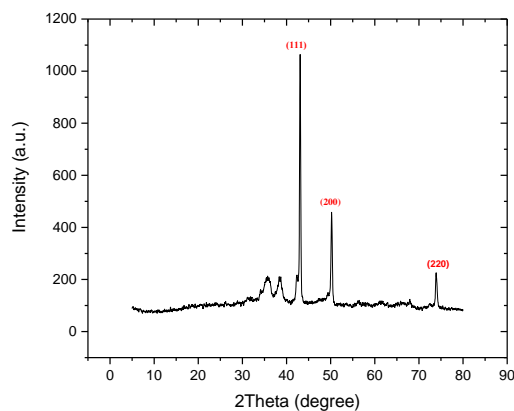


Fig. 4:- XRD pattern of Cu- NPs synthesized at 30 A via the double arc method.

Table 2:- The X-ray parameters of Cu- NPs at 30 A.

Diffraction angles(2θ) degree	I/I ₀	(h k l) Miller indices	Type	Structure	FWHM Degree	Grain size (D) (nm)
43.05	706	111	Cu	Face centered cubic	0.25630	33.32
50.18	263	200	Cu	Face centered cubic	0.28710	30.55
73.88	113	220	Cu	Face centered cubic	0.28370	35.04

The previous formulas are used in the calculation of the expected 2θ positions of the first three Cu characteristic peaks in the diffraction pattern and the interplanar spacing d for each peak. All the above parameters are listed in Table3.

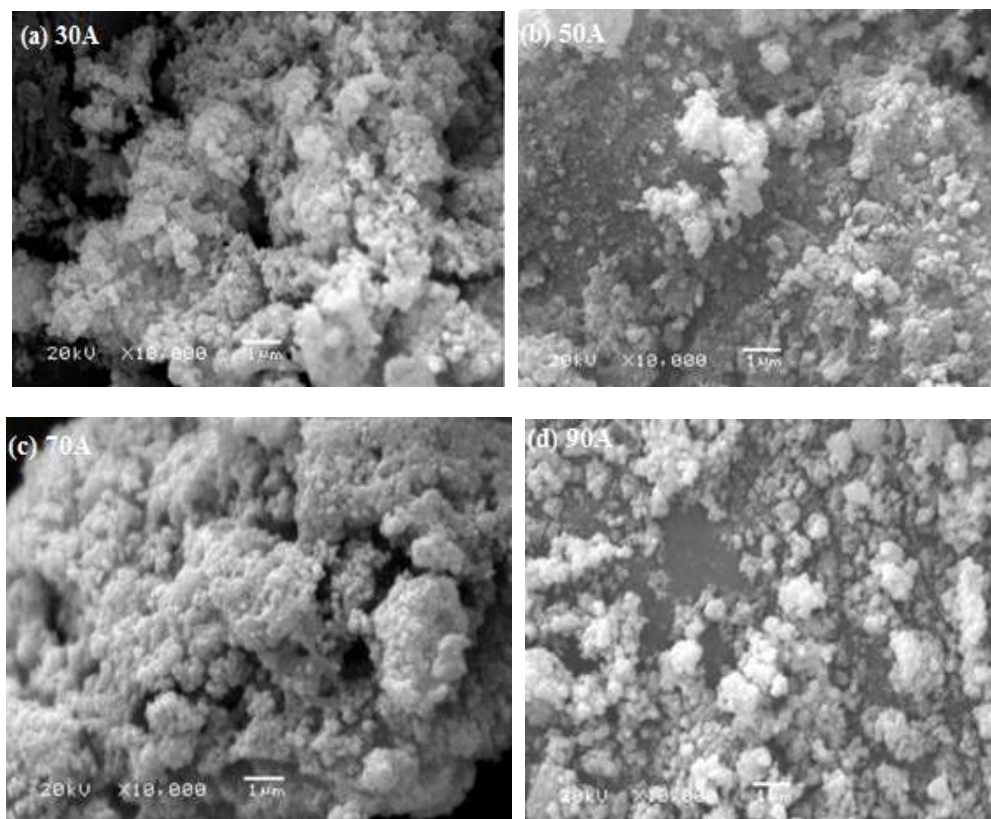
Table 3:- XRD three characteristic peaks calculated, d -Spacing and the expected 2θ positions.

2θ Measured	d -Spacing corresponding value	The expected 2θ positions
$43 \cdot 04^{\circ}$	0.21004	$43 \cdot 5^{\circ}$
$50 \cdot 18^{\circ}$	0.18170	$50 \cdot 6^{\circ}$
$73 \cdot 88^{\circ}$	0.1282	$74 \cdot 5^{\circ}$

There are 4 atoms per unit cell in the FCC cell of Cu NPs crystal structure. The density (ρ) can then be found 2.54 g/cm^3 .

SEM Analysis:-

SEM results indicate that the less miscible, arc-fabricated, brown powders are made of pure Cu NPs, which appear as spherical particles Fig. 5. These SEM images indicate the evidence of nanostructure; prior to the double arc discharge. The visual inspection of the SEM images shows conspicuous current effects on the yield, size, and morphology of Cu NPs. Accordingly, in the deionized water, 30 A is rather the best current which produce the size-selected, single crystalline Cu NPs with the average size of 34nm. SEM results show that increasing the current enlarges mean-sizes of the Cu NPs.



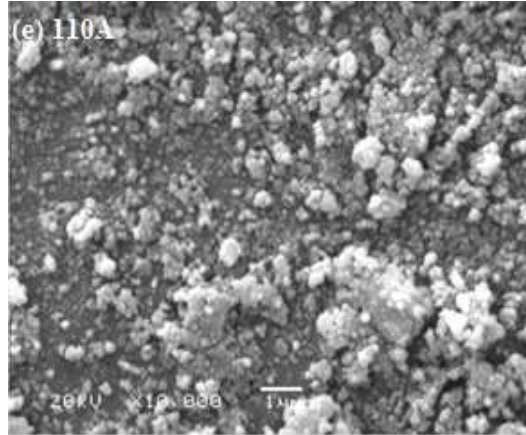


Fig. 5:- SEM images showing the influence of the arc discharge current on agglomerate structure and primary particle size of Cu NPs at a) 30A, b) 50A, c) 70A, d) 90A and e) 110A.

Obviously, the higher arc currents increase the rate of electrodes erosion, causing an increase in the macro particle formations [40]. With increasing the current the size of copper Cu NPs increases until reaching to 110A the size still increases while the yield of NPs drops and the average of Cu NPs became more than 100 nm. As a result, the sizes of Cu NPs are directly proportional to the currents employed Fig. 6. Also, the evaporation rate behaves as expected, which show that the arc increases the particle evaporation rate by increasing the electric current value Fig. 7. The combination of the two arcs discharge current is directly proportional to the Material evaporation rate. While changing current has significant effects on the particle size, it does not show any noticeable impact on the Cu NPs compositions. An increase of the arc current results not only in the growth of the agglomerate size, but also in the growth of the primary particle size. The micrograph also demonstrates that as-synthesized Cu NPs have a lot of agglomerations this is due to their small sizes and their high charge. SEM results show shows that the primary particles have a rather broad size distribution. This is due to the higher rate of vaporization of copper atoms at higher currents, making the growth rate of particles higher leading to larger particle size [41] as shown in Fig. 8.

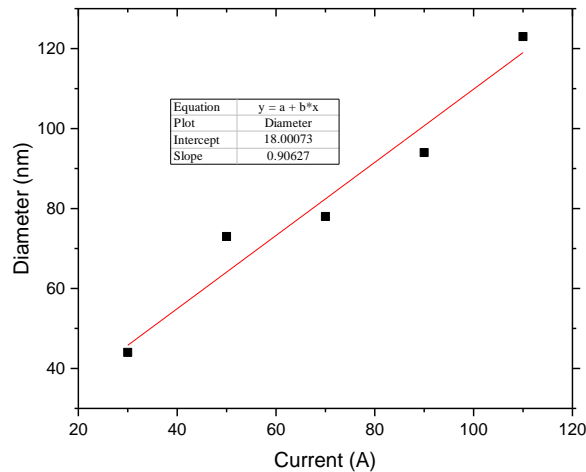


Fig. 6:- Variation of Cu NPs diameter as a function of employed currents (30–110 A).

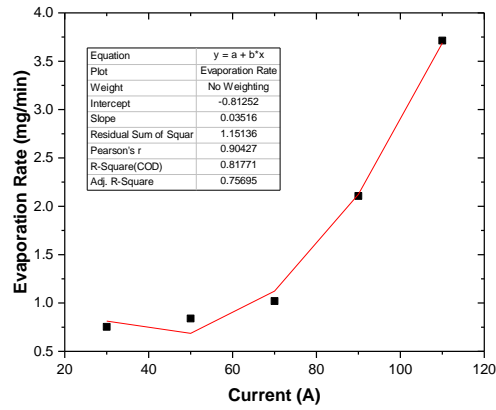


Fig. 7:- Dependence of evaporation rate on the current value.

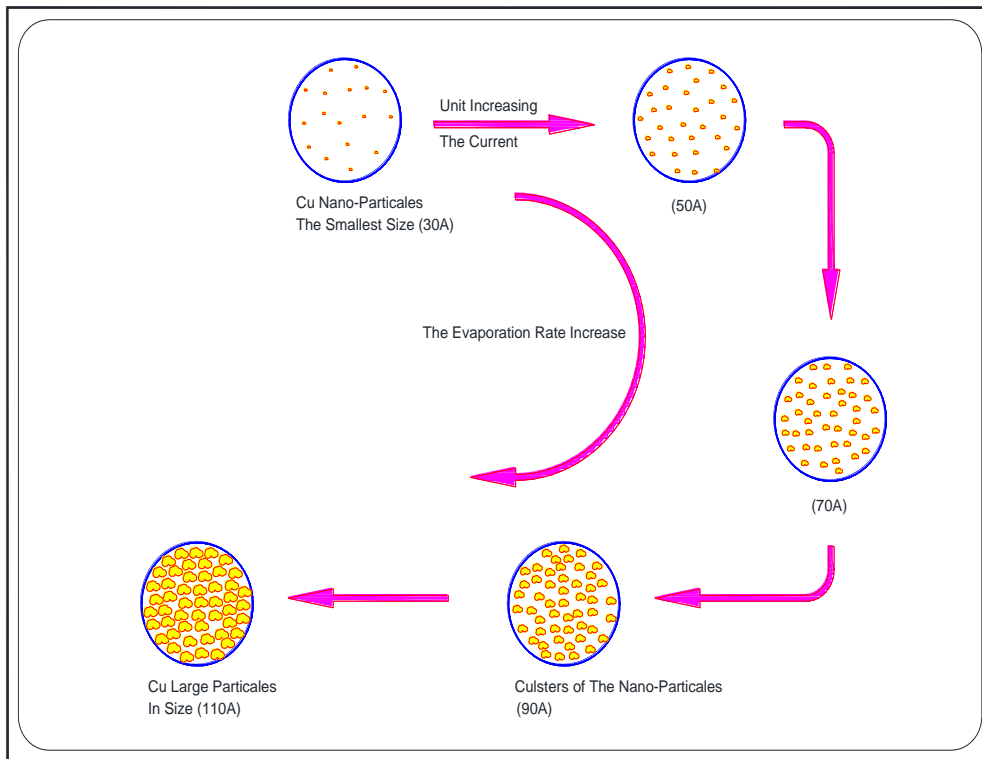
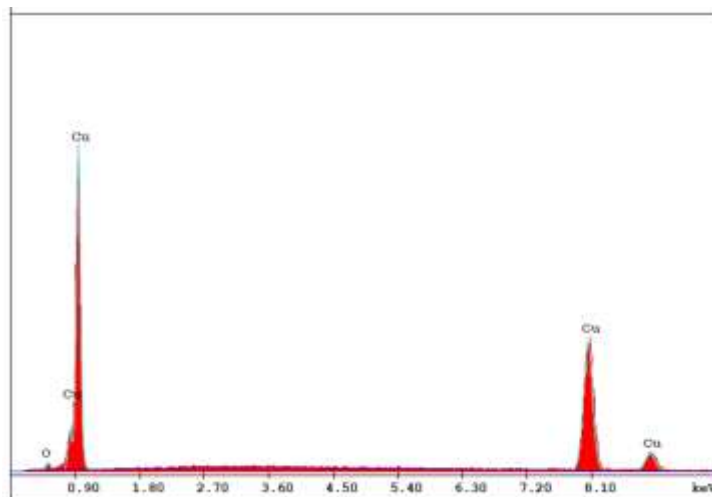


Fig.8:- Schematic diagram through the production of Cu NPs.

EDX of Cu NPs:-**Fig. 9:-** EDX of Cu NPs at 30A.

EDX can give clear information about the elements present in the samples. Fig. 9 plot not only identifies the elements corresponding to each of its peaks, but the type of X-ray to which it corresponds as well. The higher a peak in a spectrum, the more concentrated the element is in the spectrum. A large peak corresponding to copper and in addition a small scarce peak of oxygen is observed in the EDX spectrum due to that the preparation occurred in deionized water medium. Spherical shaped morphology is observed in the micrograph of Cu NPs. The dried powder of the sample was analyzed on EDX technique. It is confirmed from the EDX analysis that the grown nanoparticles are composed mainly of copper formed by double arc method. The weight percentage of Cu- NPs is more than 95%. Due to the SPR, Cu NPs shows the absorption peaks of higher counts [42]. In these spectra there are number of sharp peaks that indicate that Cu- NPs were prepared.

Particle Size Analysis:-

Particle size distribution was analyzed to make sure that the most accurate range of the Cu- NPs size is at the larger current value 110A see Fig. 8. The size distribution of the nanoparticles which is given by all the samples clarifies the average size of nanoparticles at each current which is in good agreement with SEM image analysis. Furthermore, the size distributions of the particles were obtained by analyzing the scattering profiles and the average diameters gave an indication for the size distribution of the samples with the mean average sizes.

Table 4:- Size distribution analysis of Cu NPs at different current values.

Current value	Mean Diameter (nm)
30A	9
50A	21.0
70A	45.7
90A	84.3
110A	158.2

Once nuclei are formed, they tend to aggregate in order to decrease the total surface energy. This aggregation, which can be a consequence of attractive Van der Waals forces between crystals, should be inhibited or limited to restrict the final particle size at the nanometric scale. Comparison of Fig.9 with Fig.5 shows that the Cu- NPs synthesized at 110A have a wider range of size distribution. In addition, the nanoparticles were agglomerated in these conditions while Cu- NPs synthesized at 30A are well dispersed with an average size about 34 nm. Rate of growth and agglomeration as well as nucleation of Cu- NPs. accelerated almost coincidence with the increasing of the evaporation rate. These phenomena result in the formation of nanoparticles with higher averaged size of the copper particles were precipitated (sample listed in table 4). Therefore, moderate temperature should be selected to synthesis of the nanoparticles with appropriate controlling on the size. When the copper ion evaporation rate increases with time, both the average particle size and particle size distribution increase significantly, the average particle size increased and the particle distribution remained with wide ranges.

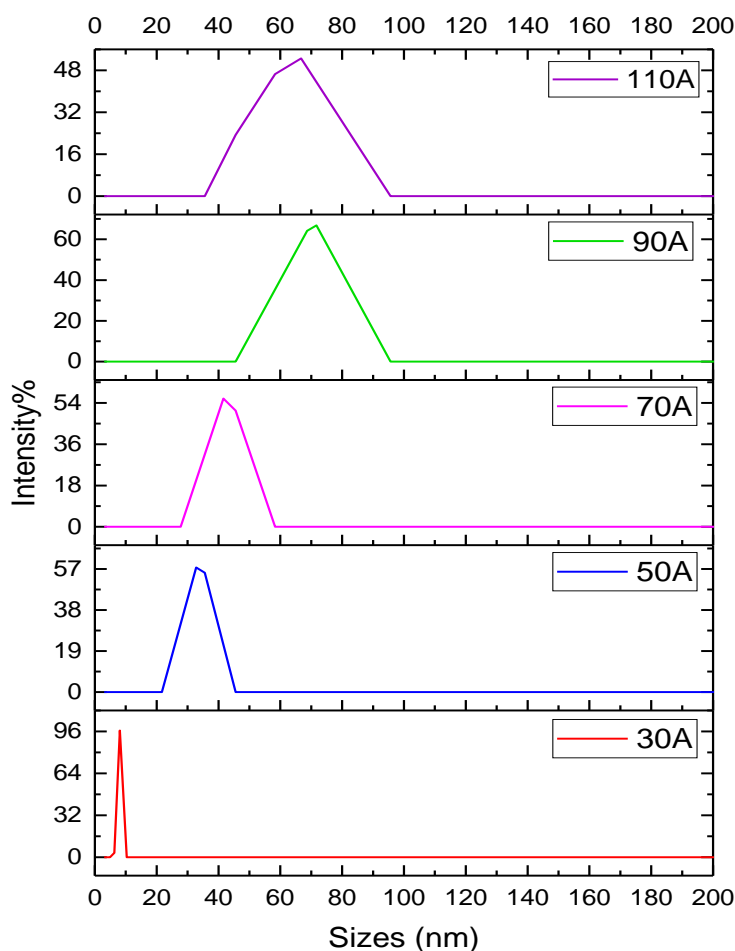


Fig. 9:- Size distribution diameters populations of Cu- NPs at 30A, 50A, 70A, 90A and 110A.

(UV-Vis) Analysis:-

Optical properties description:-

UV-visible spectra of fresh-prepared crystalline Cu- NPs samples display only unstructured absorption corresponding to small and large metal particles at different values of studying current. XRD and SEM show that the major part of Cu- NPs that are very small in size are at 30A current value (34 nm) and the other large values of current has the form of more big particles ranges (>50 nm) and more yield range. These aggregates do not have specific signals in electronic spectra in accordance with the literary data. According to Refs [43-44] only highly dispersed copper particles possess discrete signals in UV-visible range. XRD and SEM measurements revealed that part of big particles of copper was aggregated into larger ones with increasing the current (50-128 nm) [45]. The UV-Visible absorption spectrum recorded for Cu- NPs at all current values in the wavelength region 200 to 1100 nm, shown in Fig. 10 this absorption band can be attributed to the plasma resonance absorption of the copper particles. The strong surface Plasmon may be due to the formation of non-oxidized Cu- NPs. In general, the nanosized copper particles typically exhibit a surface Plasmon peak at around this range of the wavelength [46]. The surface Plasmon band at this range indicates the existence of Cu- NPs which proves the formation of the Cu- NPs in the solution [47, 48].

It was observed that the peak in the absorbance spectra increases at the beginning current value. It is due to the fact that decreasing the current value (30A) weakens the interaction force between individual nanoparticles and results in more dispersion of nanoparticles. At higher current value, the absorption peak position has changed, the absorbance peak decreases and shifting to higher wave length. But increasing the current will increase the evaporation rate and

also the number of Cu- NPs which results in higher absorbance values. It is observed that absorbance peak will increase on increasing the current value which suggests the appearance of large clusters or nanoparticles [49].

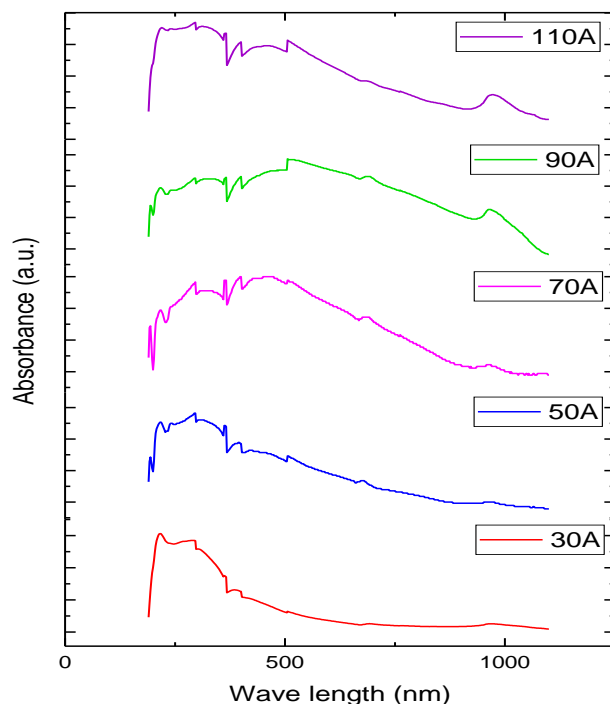


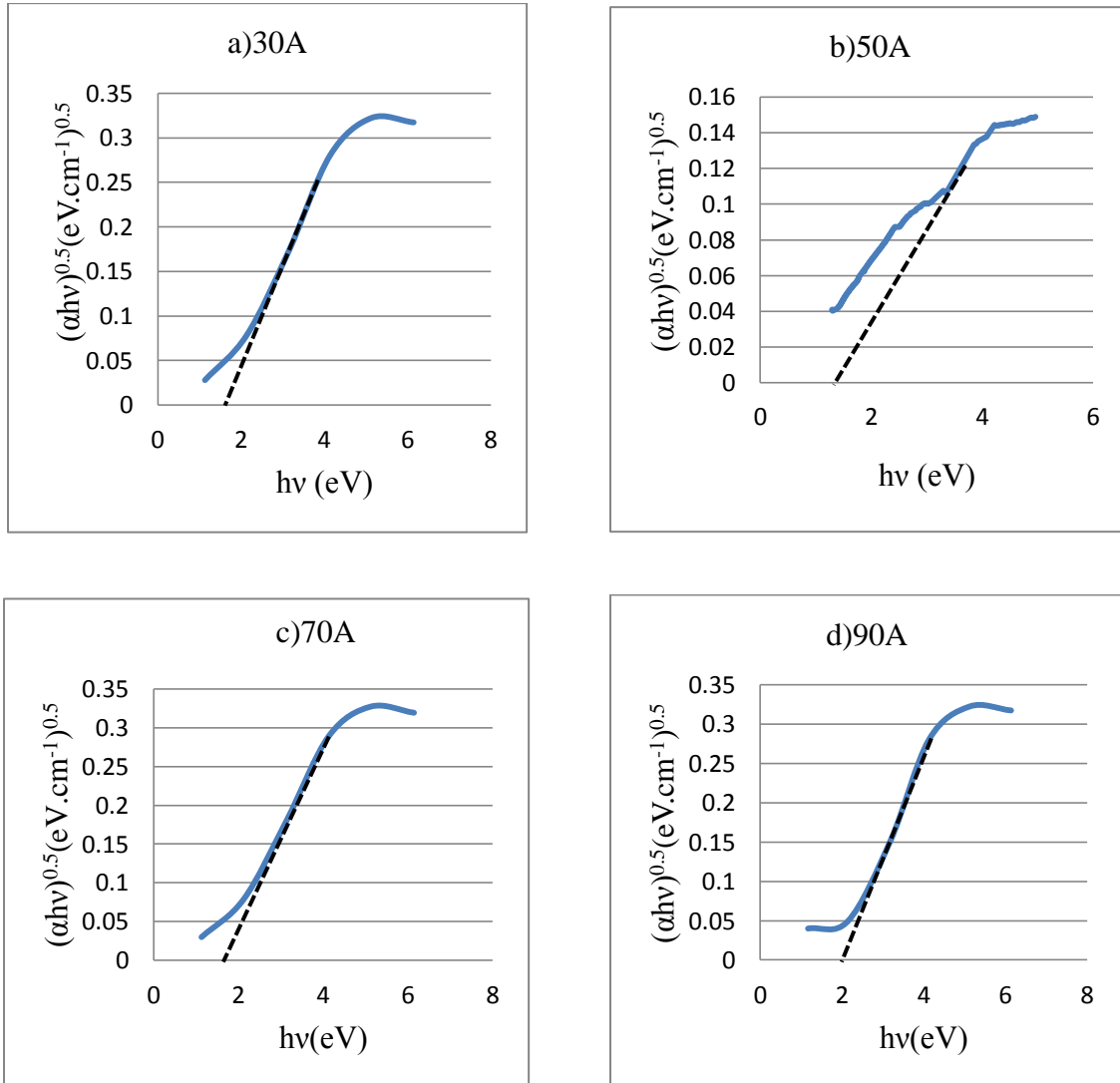
Fig. 10:- The UV-Vis absorption spectra of synthesized Cu- NPs at different currents (30- 110A).

The UV-Vis spectrophotometer (at a region about 200-1100 nm) exhibits an intense peak in between 220 and 590 nm. This peak is due to interband transition of copper electron from upper level of valence band, which is also known as surface Plasmon resonance (SPR) peak. The SPR of colloidal Cu- NPs reported previously with a peak at 220 and 590 nm is in compatible with the present result, and we can see that when the pulsed laser increases the intensity of SPR increases. where particles are large, we observe a peak position at a longer wavelength. Increased evaporation rates lead to bigger primary particles and broader agglomerate size distributions [50, 51]. The absorption peaks broad enough. This can be due to the dispersive nature of the size variation of the nanoparticles. The optical properties of copper nanocrystals [52,53] in solution have been reported. In the case of the copper nanocrystals (a few nm in size), the dipolar Plasmon resonance was found to be dependent on the shape (triangular prisms, elongated particles, cylinders, and spheres) of the copper nanocrystals. In this work, we examine the optical properties of surface confined Cu- NPs fabricated by double arc method. The deposited metal thickness (d_m), the geometry and interparticle spacing of the Cu- NPs can be controlled and the localized surface plasmon resonance LSPR can be systematically tuned throughout the visible region. Fig.10 illustrates a representative UV spectrum for a freshly prepared sample. The LSPR of the sample is very broad and the peak intensity is small. This spectral pattern was consistently observed for different samples prepared with various diameters of nanoparticles. We may note that SPR wavelength depends on size, shape of metal nanoparticles [54, 55]. Optical absorption peak is due to localized surface plasmon resonance (LSPR) for colloidal metal nanoparticles.

Energy Gap Calculations of Cu- NPs:-

The optical absorption spectrum was used to study the optical properties of the synthesized Cu- NPs; from this the band gap and the type of electronic transitions were determined. When a semiconductor absorbs photons of energy larger than the gap of the semiconductor, an electron is transferred from the valence band to the conduction band there occurs an abrupt increase in the absorbency of the material to the wavelength corresponding to the band gap energy. The relation of the absorption coefficient (α) to the incident photon energy depends on the type of electronic transitions. When in this transition, the electron momentum is conserved, the transition is direct, but if the momentum does not conserve this transition it must be attended by a photon this is an indirect electronic transition

[56]. An important feature of an energy band diagram, which is not included on the simplified diagram, is whether the conduction band minimum and the valence band maximum occur at the same value for the wavenumber. If so, the energy band gap is called direct. If not, the energy band gap is called indirect. This distinction is of interest for optoelectronic devices since direct bandgap materials provide more efficient absorption and emission of light [57, 58]. Optical absorption property of Cu- NPs can be investigated from the UV-Visible absorption spectroscopy. The energy gap of the synthesized Cu- NPs was calculated using Tauc equation. The transition data enables the best linear fit in the band edge region ($n = 1/2$ and $n = 2$). Plot of $(\alpha h\nu)^2$ vs $h\nu$ is shown in Fig. 11 and 12 respectively. The band gap values which were calculated for indirect and direct transitions are shown in Table 5.



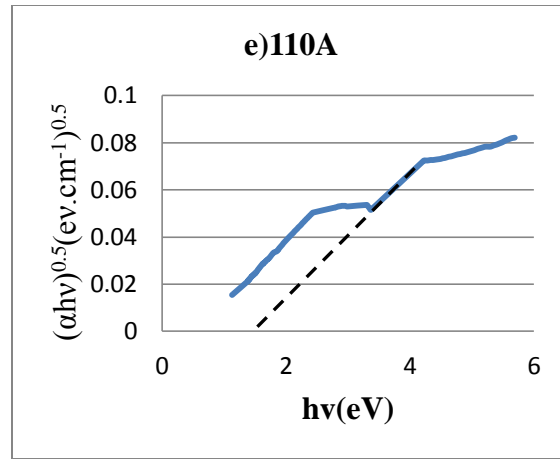
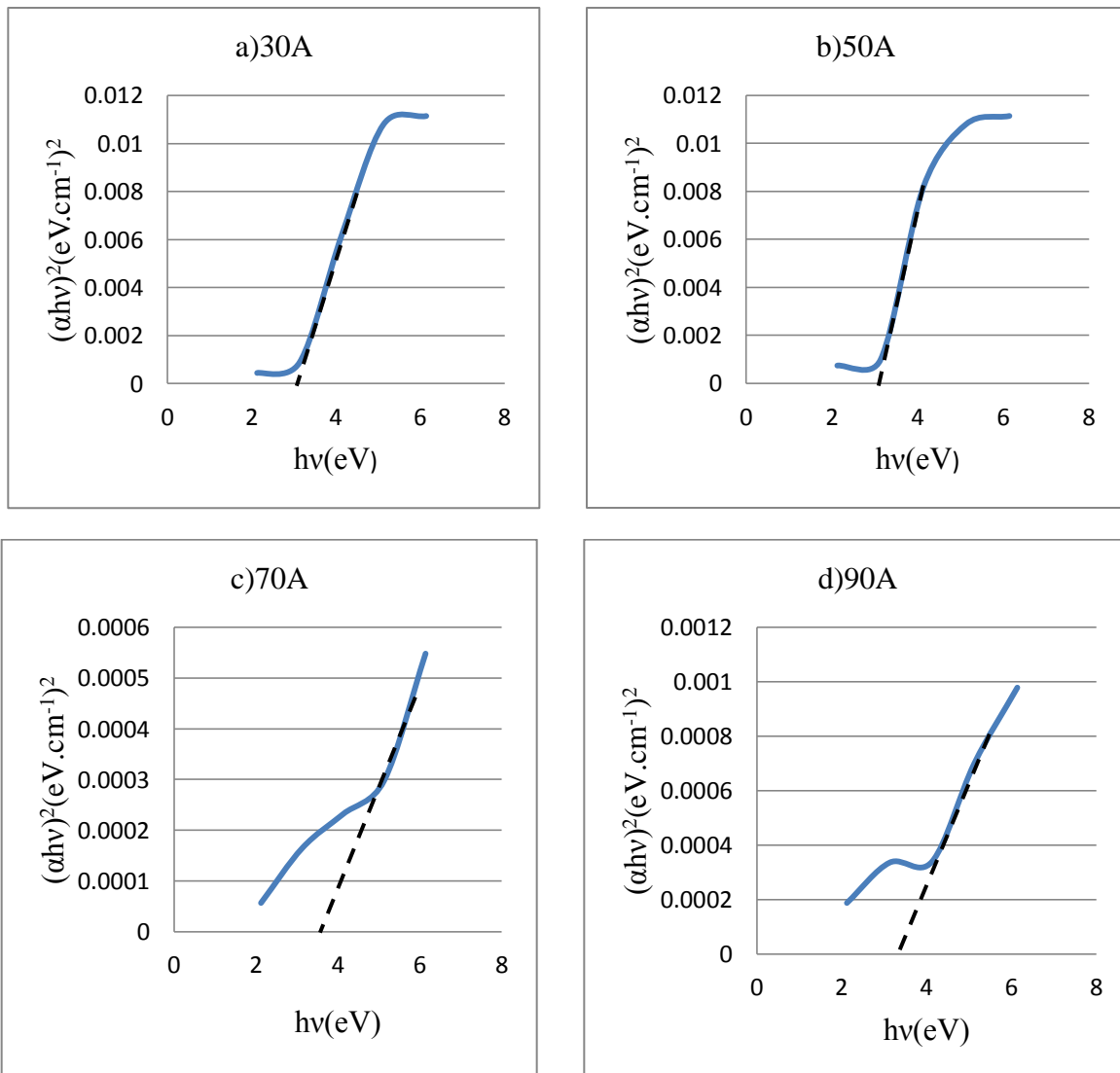


Fig. 11:-Plot from UV-Vis data to determine Energy gap of synthesized Cu- NPs at current values (30-110A).



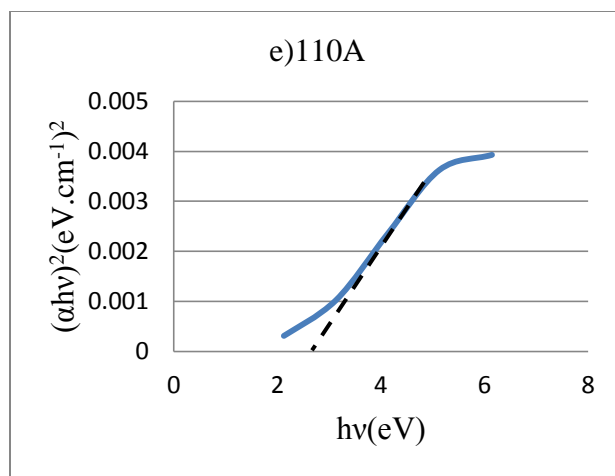


Fig. 12:- Plot from UV-VIS data to determine Energy gap of synthesized Cu- NPs at current values (30-110A).

Table 5:-Energy gap values for direct and indirect transitions.

current values	energy gap values ($n = 0.5$)	energy gap values ($n = 2$)
30A	1.2eV	3eV
50A	1.3eV	3eV
70A	1.5eV	3.2eV
90A	1.8eV	3.1 eV
110A	1.5eV	2.3eV

Tauc's plot for direct and indirect electronic transitions of Cu NPs is a functional relationship between αhv and photon energy for Cu NPs is presented. The E_g value can be obtained by extrapolating the linear portion to the photon energy axis. The values of direct and indirect band gap indicate that the material is crystalline. The optical energy gap of the Cu nano powder was found to be 2.5 eV. This value of the energy gap is consistent with that of 2.60 eV reported by Liu et al. [59] and that of 2.75 eV reported by Zhang et al. [60].

FTIR Analysis:-

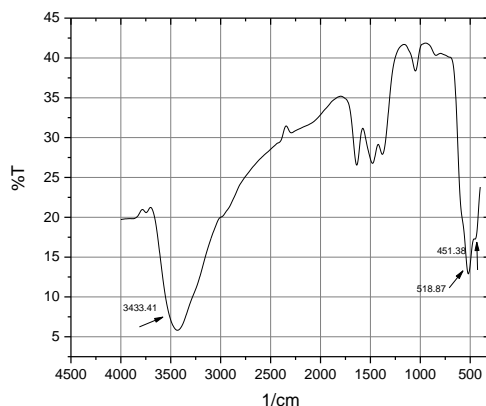


Fig.13:- FTIR spectrum of Cu- NPs at 30A.

The FTIR transmission spectrum of Cu- NPs at 30 A is shown in Fig.13. It can be observed that the bands at 451.38 cm^{-1} and 518 cm^{-1} were assigned to be symmetric and asymmetric stretching modes of vibration metal. The broad absorption peak at 3426 cm^{-1} indicates the presence of hydroxyl group which represents the water as moisture in the

sample. The FTIR spectrum of the sample confirms the absence of any other residual organic compound. It is prominent that no infrared active modes from Cu NPs were detected which is in good agreement with the XRD results.

Conclusion:-

In summary, stable and pure three-phase double-arc discharge system presented is easy to construct, simple and inexpensive to operate and fabricate Cu NPs in a very small size. The double arc discharges which was submerged in dielectric liquid was found to be suitable for the production of Cu NPs. Different values of currents (30, 50, 70, 90 and 110A) are passed through Cu electrodes. It produces different size ranges of the Cu nanoparticles in each single arc. In this experiment, a new technique of discharge under liquid surface have been successfully applied for the synthesis of copper and different types of metals which is called double arc discharge method. Spherical Cu NPs were prepared by a novel synthesis technique which is simple and environmentally benign. It is an easy, fast technique and doesn't involve any harmful or toxic chemicals. It is also stable and accurate enough to be applied at different ranges of currents. The double arc discharges which were submerged in dielectric liquid is suitable to produce Cu- NPs. The structural analysis by XRD, SEM, EDX, P.S, UV-Vis and FTIR is confirmed that the synthesis of copper NPs was stable. The experiments suggested the possibility of using different types of materials in order to prepare many different structures of NPs.

References:-

1. Montaser A, Golightly DW (1992) Inductively Coupled Plasmas in Analytical Atomic Spectrometry. VCH Publishers Inc. New York
2. Mohamed MM (1989) Ph.D. Thesis, Osaka University, Japan
3. Park SJ, Lazarides AA, Mirkin, CA, Letsinger RL (2001) Directed Assembly of Periodic Materials from Protein and Oligonucleotide-Modified Nanoparticle Building Blocks. *Angewandte Chemie International Edition* 40(15):2909-2912
4. Ponce AA, labunde KJ (2005) Chemical and catalytic activity of copper nanoparticles prepared via metal vapor synthesis. *Journal of Molecular Catalysis A* 225 (1):1-6
5. Pferiffer T V, Feng J, Schmidt-ott A (2004) New development in spark production of nanoparticles 25(1):56-70
6. Siegel, Richard W, Evelyn Hu, eds(1999) Nanostructure Science and Technology: R & D Status and Trends in Nanoparticles, Nanostructured Materials and Nanodevices. Springer Science & Business Media
7. Nehra V, Kumar A, Dwivedi HK (2008) Atmospheric non-thermal plasma sources. *International Journal of Engineering* 2(1):53-68
8. Yao WT, Yu SH, Zhou Y, Jiang J, Wu QS, Zhang L, Jiang J(2005). Formation of uniform CuO nanorods by spontaneous aggregation Selective synthesis of CuO, Cu₂O, and Cu nanoparticles by a solid- liquid phase arc discharge process. *The Journal of Physical Chemistry B*(29):14011-6
9. Qin C, Coulombe S(2007) Organic layer-coated metal nanoparticles prepared by a combined arc evaporation/condensation and plasma polymerization process. *Plasma Sources Science and Technology* (2):240
10. Mallikarjuna K, Narasimha G, Dillip GR, Praveen B, Shreedhar B, Lakshmi CS, Reddy BV, Raju BD (2011) Green synthesis of silver nanoparticles using Ocimum leaf extract and their characterization. *Digest Journal of Nanomaterials and Biostructures*6(1):181-6
11. Keidar M, Levchenko I, Arbel T, Alexander M, Waas AM, Ostrikov KK (2008). Magnetic-field-enhanced synthesis of single-wall carbon nanotubes in arc discharge. *Journal of Applied Physics* 103(9):094318
12. Akita S, Kamo S, Nakayama Y (2002) Diameter control of arc produced multiwall carbon nanotubes by ambient gas cooling. *Japanese journal of applied physics* 41(4): L487
13. Tsuruoka T, Kumazaki S, Osaka I, Nawafune H, Akamatsu K (2013). Synthesis of Polystyrene-based Nanocomposite Thin Films with Domain Structure Consisting of Au Nanoparticles. In *Journal of Physics: Conference Series* (Vol. 417, No. 1, p. 012020). IOP Publishing.
14. Xie SY, Ma ZJ, Wang CF, Lin SC, Jiang ZY, Huang RB, Zheng LS (2004) Preparation and self-assembly of copper nanoparticles via discharge of copper rod electrodes in a surfactant solution a combination of physical and chemical processes. *Journal of Solid State Chemistry* 177(10):3743-7
15. Rahaghi SH, Poursalehi R, Miresmaeili R (2015) optical properties of Ag-Cu alloy nanoparticles synthesized by DC arc discharge in liquid. *Procedia Materials Science* (11) 738-42

16. Tendero C, Tixier C, Tristant P, Desmaison J, Leprince P (2006) Atmospheric pressure plasmas. *Atomic Spectroscopy* 61(1):2-30
17. Celik C, Addona T, Boulos MI, Chen G, Davis HJ, inventors; Noranda Inc, assignee. Method and transferred arc plasma system for production of fine and ultrafine powders. United States patent US 6,379,419. 2002 Apr 30
18. Mahoney W, Andres RP (1995) Aerosol synthesis of nanoscale clusters using atmospheric arc evaporation. *Materials Science and Engineering* 204(1-2):160-4
19. Förster H, Wolfrum C, Peukert W (2012) Experimental study of metal nanoparticle synthesis by an arc evaporation/condensation process. *Journal of Nanoparticle Research*: 14(7):926
20. Munz RJ, Addona T, da Cruz AC (1999) Application of transferred arcs to the production of nanoparticles. *Pure and Applied Chemistry* 71(10):1889-97
21. Lee JG, Li P, Choi CJ, Dong XL (2010) Synthesis of Mn–Al alloy nanoparticles by plasma arc discharge. *Thin Solid Films* 519(1):81-5
22. Kassaei MZ, Buazar F (2009) Al nanoparticles impact of media and current on the arc fabrication. *Journal of manufacturing processes* 11(1):31-7
23. Scott JH, Majetich SA (1995). Morphology, structure, and growth of nanoparticles produced in a carbon arc. *Physical Review B* 52(17):12564
24. Švarcová S, Kočí E, Bezdička P, Hradil D, Hradilová J (2010). Evaluation of laboratory powder X-ray micro-diffraction for applications in the fields of cultural heritage and forensic science. *Analytical and bioanalytical chemistry* 398(2):1061-76.
25. Langford JI, Wilson AJ (1978) Scherrer after sixty years: a survey and some new results in the determination of crystallite size. *Journal of Applied Crystallography* 11(2):102-13
26. Shokr M. Pn CCD Response to Hard X-Ray Radiation. LAP LAMBERT Academic Publishing; 2016
27. Jores K, Mehnert W, Drechsler M, Bunjes H, Johann C, Mäder K (2004) Investigations on the structure of solid lipid nanoparticles (SLN) and oil-loaded solid lipid nanoparticles by photon correlation spectroscopy, field-flow fractionation and transmission electron microscopy. *Journal of Controlled Release* 95(2):217-27
28. McHale R, Liu Y, Ghasdian N, Hondow NS, Ye S, Lu Y, Brydson R, Wang X (2011) Dual lanthanide role in the designed synthesis of hollow metal coordination (Prussian Blue analogue) nanocages with large internal cavity and mesoporous cage. *Nanoscale* 3(9):3685-94
29. Redhead, HM, Davis, SS, Illum, L (2001) Drug delivery in poly (lactide-co-glycolide) nanoparticles surface modified with poloxamer 407 and poloxamine 908: in vitro characterisation and in vivo evaluation. *Journal of Controlled Release* 70(3):353-363
30. Ting CC, Chen SY, Liu DM (2000) Structural evolution and optical properties of TiO₂ thin films prepared by thermal oxidation of sputtered Ti films. *Journal of Applied Physics* Oct 88(8): 4628-33
31. Cohen M, Chelikowsky J (2012) *Electronic structure and optical properties of semiconductors* 75. Springer Science & Business Media.
32. López-Romero S, Castillo-Mendoza SJ, Chávez-Ramírez J, Díaz-Becerril K (2003) Síntesis y caracterización óptica, eléctrica y estructural de películas delgadas de CS₂ depositadas por el método PECVD. *Materia* 8(4):341-9
33. Oliva FY, Avalle LB, Santos E, Cámara OR (2002) Photoelectrochemical characterization of nanocrystalline TiO₂ films on titanium substrates. *Journal of photochemistry and photobiology A. chemistry* 146(3):175-88
34. Zavyalov SA, Timofeev AA, Pivkina AN, Schoonman J (2004) Metal-polymer Nanocomposites: Formation and Properties Near the Percolation Threshold. In *Nanostructured Materials* Springer, Boston, MA. (97-113)
35. Lushnikov AA, Simonov AJ (1974) Surface plasmons in small metal particles. *Zeitschrift für Physik* 270(1):17-24
36. Mie G (1908). Beiträge zur Optik trüber Medien, speziell kolloidaler Metallösungen *Annalen der Physik* 330(3):377-445
37. Ritchie RH (1957) Plasma losses by fast electrons in thin films. *Physical Review* 106(5):874
38. Barnes WL, Dereux A, Ebbesen TW (2003) Surface plasmon subwavelength optics. *Nature* 424(6950):824-830
39. Mudunkotuwa IA, Al Minshid A, Grassian VH (2014) ATR-FTIR spectroscopy as a tool to probe surface adsorption on nanoparticles at the liquid–solid interface in environmentally and biologically relevant media. *Analyst* 139(5):870-81
40. Tsung TT, Chang H, Chen LC, Han LL, Lo CH, Liu MK (2003) Development of pressure control technique of an arc-submerged nanoparticle synthesis system (ASNSS) for copper nanoparticle fabrication. *Materials Transactions* 44 (6):1138-42

41. Lo CH, Tsung TT, Chen LC (2005) Ni nano-magnetic fluid prepared by submerged arc nano synthesis system (SANSS). *JSME International Journal Series B Fluids and Thermal Engineering* 48(4):750-5
42. Bindhu MR, Umadevi M (2013) Synthesis of monodispersed silver nanoparticles using Hibiscus cannabinus leaf extract and its antimicrobial activity. *Spectrochimica Acta Part A: Molecular and Biomolecular Spectroscopy* 15 (101):184-90
43. Komova OV, Simakov AV, Rogov VA, Kochubei DI, Odegova GV, Kriventsov VV, Paukshtis EA, Ushakov VA, Sazonova NN, Nikoro TA (2000) Investigation of the state of copper in supported copper–titanium oxide catalysts. *Journal of Molecular Catalysis A Chemical* 161(1-2):191-204
44. Markel VA, Shalaev VM, Zhang P, Huynh W, Tay L, Haslett TL, Moskovits M (1999) Near-field optical spectroscopy of individual surface-plasmon modes in colloid clusters. *Physical Review B*. 59(16):10903
45. Kapoor S, Joshi R, Mukherjee T (2002) Influence of I anions on the formation and stabilization of copper nanoparticles. *Chemical Physics Letters* 354(5-6):443-8
46. Zhao Y, Zhu JJ, Hong JM, Bian N, Chen HY (2004) Microwave- Induced Polyol- Process Synthesis of Copper and Copper Oxide Nanocrystals with Controllable Morphology. *European Journal of Inorganic Chemistry* 1 (20):4072-80
47. Kapoor S, Joshi R, Mukherjee T (2002) Influence of I anions on the formation and stabilization of copper nanoparticles. *Chemical Physics Letters* 354(5-6):443-8
48. Zhang HX, Siegert U, Liu R, Cai WB (2009) Facile fabrication of ultrafine copper nanoparticles in organic solvent. *Nanoscale research letters* 4 (7):705.
49. Curtis AC, Duff DG, Edwards PP, Jefferson DA, Johnson BF, Kirkland AI, Wallace AS (1988) Preparation and structural characterization of an unprotected copper sol. *The Journal of Physical Chemistry* 92(8):2270-5
50. Mahoney W, Andres RP (1995) Aerosol synthesis of nanoscale clusters using atmospheric arc evaporation. *Materials Science and Engineering A* 204(1-2):160-4
51. Link S, El-Sayed MA (2000) Shape and size dependence of radiative, non-radiative and photothermal properties of gold nanocrystals. *International reviews in physical chemistry* 19(3):409-53
52. Wang H, Tam F, Grady NK, Halas NJ (2005) Cu nanoshells: effects of interband transitions on the nanoparticle plasmon resonance. *The Journal of Physical Chemistry B* 109(39):18218-22
53. Salzemann C, Brioude A, Pileni MP (2006) Tuning of copper nanocrystals optical properties with their shapes. *The Journal of Physical Chemistry B* 110(14):7208-12
54. Kreibig, U, Vollmer, M (1995) Theoretical considerations. In *Optical Properties of Metal Clusters* (pp. 13-201). Springer Berlin Heidelberg
55. Yeshchenko OA, Dmitruk IM, Dmytruk AM, Alexeenko AA (2007) Influence of annealing conditions on size and optical properties of copper nanoparticles embedded in silica matrix. *Materials Science and Engineering* 137(1-3):247-54
56. Rehman S, Mumtaz A, Hasanain SK (2011) Size effects on the magnetic and optical properties of CuO nanoparticles. *Journal of Nanoparticle Research*: 13(6):2497-507.
57. Willardson, RK, Beer, AC eds. (1967) *Optical properties of III-V compounds*. Academic Press
58. Dressel M, Grüner G (2002). *Electrodynamics of solids optical properties of electrons in matter*: 1269-1270
59. Liu Q, Liu H, Liang Y, Xu Z, Yin G (2006) Large-scale synthesis of single-crystalline CuO nanoplatelets by a hydrothermal process. *Materials research bulletin* 41(4):697-702
60. Zhang X, Zhang D, Ni X, Zheng H (2008) Optical and electrochemical properties of nanosized CuO via thermal decomposition of copper oxalate. *Solid-State Electronics* 52(2):245-8